Parametric hybrid scattering from light-induced ferroelectric and photorefractive structures

A. Selinger, U. Voelker, V. Dieckmann, and M. Imlau

University of Osnabrück, Department of Physics, Barbarastr. 7, 49069 Osnabrück, Germany

aselinge@uos.de

M. Goulkov

Institute of Physics, Science Ave 46, 03650, Kiev-39, Ukraine

Abstract: Processes of photo-induced light scattering are studied in single crystals of $LiNbO_3$:Fe to uncover the origin of a new part of the entire scattering pattern which can be observed on a viewing screen. The new scattering manifests itself as two arcs enclosing the directly transmitting pump beam. It is shown that this type of scattering is due to a parametric wave-mixing process of coherent optical noise and a pump beam on a combination of photorefractively recorded phase-gratings and photo-induced ferroelectric structures. Phase-matching conditions corresponding to the new scattering are introduced. All photo-induced scattering phenomena contributing to the total scattering pattern are discussed, compared and classified.

OCIS codes: (190.5330) Photorefractive nonlinear optics; (160.2260) Ferroelectrics

References and links

1. *Photorefractive materials and their applications*, P. Günter and J.-P. Huignard, eds. (Springer, New York, 2005).
2. B. I. Sturman, S. G. Odoulov, and M. Yu. Goulkov, "Parametric four-wave processes in photorefractive crystals," Phys. Rep. **275,** 197–254 (1996).
3. B. Sturman, M. Aguilar, F. Agulló-López, V. Pruneri, and P. G. Kazansky, "Photorefractive nonlinearity of periodically poled ferroelectrics," J. Opt. Soc. Am. B **14,** 2641–2649 (1997).
4. M. Goul'kov, S. Odoulov, I. Naumova, F. Agulló-López, G. Calvo, E. Podivilov, B. Sturman, and V. Pruneri, "Degenerate parametric light scattering in periodically poled $LiNbO_3$:Y:Fe," Phys. Rev. Lett. **86,** 4021–4024 (2001).
5. U. Hartwig, M. Kösters, Th. Woike, K. Buse, A. Shumelyuk, and S. Odoulov, "Frequency mixing of photorefractive and ferroelectric gratings in lithium niobate crystals," Opt. Lett. **31,** 583–585 (2006).
6. M. Kösters, U. Hartwig, Th. Woike, K. Buse, and B. Sturman, "Quantitative characterization of periodically poled lithium niobate by electrically induced Bragg diffraction," Appl. Phys. Lett. **88,** 182910 (2006).
7. S. A. Basun, A. A. Kaplyanskiĭ, and S. P. Feofilov, "Light induced three-dimensional polar structure in ruby crystals," JETP Lett. **37,** 586–589 (1983).
8. A. S. Kewitsch, M. Segev, A. Yariv, G. J. Salamo, T. W. Towe, E. J. Sharp, and R. R. Neurgaonkar, "Ferroelectric domain gratings in strontium barium niobate induced by photorefractive space charge fields," Phys. Rev. Lett. **73,** 1174–1177 (1994).
9. A. S. Furman, "Photoelectric domains in para- and ferroelectrics," JETP Lett. **41,** 216–220 (1985).
10. V. V. Lemeshko and V. V. Obhukhovsky, "Domains in photoexcited $LiNbO_3$:Fe," Sov. Phys. Solid State **30,** 1614–1618 (1988).
11. M. Goulkov, S. Odoulov, Th. Woike, J. Imbrock, M. Imlau, E. Krätzig, C. Bäumer, and H. Hesse, "Holographic light scattering in photorefractive crystals with local response," Phys. Rev. B **65,** 195111 (2002).

#78429 - $15.00 USD Received 22 Dec 2006; revised 23 Mar 2007; accepted 26 Mar 2007; published 3 Apr 2007

12. V. V. Voronov, I. R. Dorosh, Yu. S. Kuz'minov, and N.V. Tkachenko, "Photoinduced light scattering in cerium-doped barium strontium niobate crystals," Sov. J. Quantum Electron. **10,** 1346–1349 (1980).
13. J. Feinberg, "Asymmetric self-defocusing of an optical beam from the photorefractive effect," J. Opt. Soc. Am. **72,** 46–51 (1982).
14. K. G. Belabaev, I. N. Kiseleva, V. V. Obukovskiĭ, S. G. Odulov, and R. A. Taratuta, "New parametric holographic-type scattering of light in lithium tantalate crystals," Sov. Phys. Solid State **28,** 321–322 (1986).
15. D. S. Smith, H. D. Riccius and R. P. Edwin, "Refractive indices of lithium niobate," Opt. Commun. **17,** 332–335 (1976).
16. B. I. Sturman, "Low-frequency noise and photoinduced light scattering in photorefractive crystals," JETP **73,** 593–595 (1991).
17. D. D. Cooke and M. Kerker, "Light scattering from long thin glass cylinders at oblique incidence," J. Opt. Soc. Am. **59,** 43–48 (1969).
18. Q. Li and D. Feng, "Domain structures induced by defects in $Ba_2NaNb_5O_{15}$ and $LiNbO_3$," Ferroelectrics **97,** 217–226 (1989).
19. K. G. Deshmukh and K. Singh, "Interferometric study of the microtopography arising from 35° domain walls in crystals of lithium niobate," J. Phys. D: Appl. Phys. **97,** 1321–1323 (1973).
20. I. I. Naumova, N. F. Evlanova, O. A. Gliko, and S. V. Lavrichev, "Czochralski-grown lithium niobate with regular domain structure," Ferroelectrics **190,** 107–112 (1997).

1. Introduction

This contribution is devoted to a new type of parametric multi-wave mixing on a combination of photorefractive gratings and ferroelectric polar structures both induced by a single laser pump beam in photosensitive ferroelectrics. The study is performed with the nonlinear optical phenomenon of photo-induced light scattering (PILS) in *a*-cut samples of single-domain $LiNbO_3$:Fe. The crystal is characterized by a pronounced photorefractive effect, which is utilized for the recording of volume phase gratings in many optical applications [1]. During the recording, spatial light variations originating from coherent wave interference are transferred into electric space-charge fields which change the refractive index via the linear electrooptic effect. The mixing of recording waves on photorefractive gratings is followed by energy and/or phase changes [1]. The PILS phenomenon is the result of different wave mixing processes between scattered and transmitted parts of the pump beam on noisy photorefractive gratings. This is why a large number of such processes can be observed and studied particularly with the help of the PILS phenomenon [2]. Usually, wave mixing is investigated with photorefractive gratings. In a few recent works, the influence of ferroelectric gratings on the wave mixing was elucidated with periodically poled $LiNbO_3$:Fe as an example [3, 4, 5]. Spatially altered ferroelectric domains which result either from a special growing technique or from purposive manipulations, e.g. by externally applied electric fields, enable light diffraction from domain walls [6]. It is also reported that microscopic domains structures can be induced by coherent illumination in some materials [7, 8]. For lithium niobate the effect of photo-assisted nucleation of ferroelectric domains was first theoretically predicted [9], and then experimentally observed in thin *c*-cut $LiNbO_3$:Fe samples via scattering cones oriented along the **c**-axis [10]. 180°-domains were induced on the *c*-surface by high electric fields. The fields are due to the photovoltaic effect, which is the main electric charge-transport mechanism in this material. It was shown that exhaustive information about light-induced domains can be retrieved by studying the scattering process. However, the discovered effect was not due to any wave mixing which could further result in an effective light amplification.

We report on parametric multi-wave mixing on the combination of photorefractive gratings together with bulk variations of the ferroelectric domain structure all induced by one pump beam of moderate intensity. This complicate mixing of coherent noise and the pump beam results in a parametric hybrid PILS process observed in *a*-cut $LiNbO_3$:Fe crystals and manifests itself as two scattering arcs opened in the direction towards the pump beam on a viewing screen. The pattern appears on the background of other PILS phenomena. The discussion and

#78429 - $15.00 USD Received 22 Dec 2006; revised 23 Mar 2007; accepted 26 Mar 2007; published 3 Apr 2007

classification therefore will be done for all scattering processes accompanying the discovered effect.

2. Setup

The experiment was performed with *a*-cuts of $LiNbO_3$:Fe of the congruently melting composition. The Fe_2O_3 concentration was 0.125 wt.% in the melt. The dimensions of the samples were $4 \times 5\,mm^2$ with thicknesses d in the range of $0.1 - 4$ mm. A Q-switched and a continuous-wave frequency-doubled Nd:YAG-laser system, respectively, emitting light at $\lambda = 532$ nm are used as a pump beam. Dispersive investigations were performed with an Ar^+-Kr^+-ion laser providing wavelengths in the range from 457.9 nm to 647 nm. Intensity and light polarization of the unexpanded pump beam were adjusted by a combination of a $\lambda/2$-retarder waveplate and a Glan-Thompson-polarizer. All experiments were performed with a laser intensity of $I_p = 0.2 - 0.7\,W/cm^2$ and extraordinary light polarization. The intensities of transmitted and scattered light were collected using Si-PIN photodiodes. The shape of the scattering pattern was detected on a semi-transparent screen by a charge-coupled-device-array (CCD). Polarizers have been inserted optionally between crystal and detectors providing a distinct analysis of the polarization of the scattered light. The crystal position was accurately adjusted ($\pm 0.001\,°$) by a motorized rotation stage and a goniometer. The schematic setup is presented in Fig. 1. If a defined virgin condition was required, the crystals were heated for 60 minutes at 350 °C prior to the experiments.

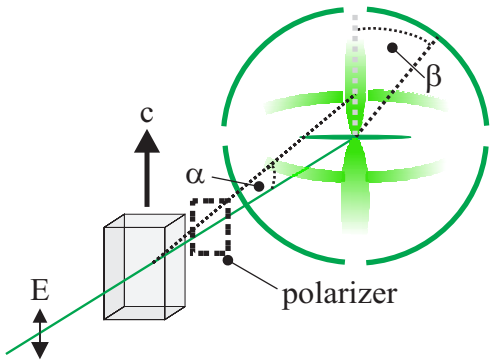

Fig. 1. Schematic illustration of the experimental setup. The apex angle α and the azimuth angle β are used to precisely describe positions on the scattering pattern

3. Results

When the samples are illuminated by a laser beam the scattering develops as a function of time and can be observed as a light pattern on the viewing screen placed behind the crystal. A polarizer between crystal and screen revealed that parts of the entire scattered light are scattered polarization-isotropically (no polarization change in respect to the pump beam) and other parts are scattered polarization-anisotropically (light polarization orthogonal to that of the pump beam). The same scattering pattern was observed in samples of different thicknesses irradiated by either pulsed or continuous-wave laser light in the spectral range from 457.9 nm to 647 nm. Figure 2(a) shows a photograph of the observed scattering pattern for the angle θ_p=90° between the pump beam and the **c**-axis of the crystal. It was taken for a $LiNbO_3$:Fe crystal ($d = 800\,\mu m$) exposed to continuous-wave laser light (λ = 532 nm, **E** $\parallel$ *c*) of an intensity of $0.5\,W/cm^2$ after an exposure time of $\geq$ 200 s, i.e. in the steady state. The polarizer behind the crystal was adjusted

#78429 - $15.00 USD Received 22 Dec 2006; revised 23 Mar 2007; accepted 26 Mar 2007; published 3 Apr 2007

in a way that all scattering patterns were visualized at the same time. The pump beam in the center is masked on the screen. Taking into account the geometry and the polarization states, the entire scattering can be separated into four distinguishable parts: i) a diffusive polarization-isotropic wide-angle scattering which appears as two lobes, one into the $+c$- and one into the $-c$- direction, symmetrically towards the pump beam; ii) a polarization-anisotropic sharp ring which has its center in the pump beam spot; iii) a polarization-isotropic line aligned horizontally through the pump beam; iv) two polarization-anisotropic slightly diffusive arcs, inner with respect to the ring and symmetrically aligned beneath and above the pump beam. Pattern iv) is a new type of scattering which was not reported before. Figure 2(b) shows a photograph of this pattern taken from a projection on a screen for a pump-beam-alignment of θ_p=77° towards the **c**-axis. The arc aligned in the direction of the crystal slant (lower on the photo) increases in curvature and moves from the pump beam, while the opposite arc moves towards the beam and flattens.

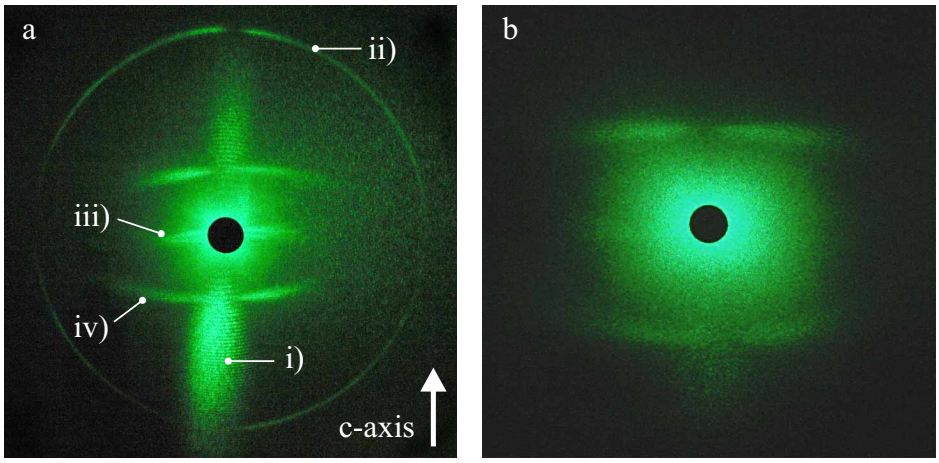

Fig. 2. Photographs of the scattering, taken from the viewing screen. a) The entire scattering pattern at normal pump beam incidence: i) polarization-isotropic lobes, ii) polarization-anisotropic ring, iii) polarization-isotropic line, iv) polarization-anisotropic arcs. b) Photograph of pattern iv) taken for oblique light incidence (θ_p=77°) with only ordinary polarized light passing the polarizer.

A geometrical investigation of the scattering pattern shows that the sharp ring possesses an angular distance of $26.9^\circ \pm 0.5^\circ$ with respect to pump beam. For the two arcs the angle in the c-plane in respect to the horizontal plane has been measured to be in the range of $(7.9 \pm 0.5 - 9.9 \pm 0.5)^\circ$ (values given for $\lambda = 532$ nm). This angular range characterizes the diffusive width of the scattering.

The intensities of the four scattering patterns develop as a function of time from the beginning of exposure as shown in Fig. 3. For comparison, the kinetics of the transmitted pump beam is given in the same figure. All intensities are normalized to the respective maximum value. The intensity of the scattering lobes (pattern i)) was monitored at an angle of $\alpha = 30^\circ$ and increases directly from the beginning. The same holds for the intensity of the polarization-anisotropic ring (pattern ii)) measured at the azimuth angle $\beta = 22.1^\circ$. The horizontal line (pattern iii)) was measured at $\alpha = 6.1^\circ$ and the upper arc (pattern iv)) at $\beta = 45.0^\circ$. The two latter patterns show a characteristic time threshold, which is reduced with increasing pump beam intensity but does not depend on the crystal thickness. All scattering signals in Fig. 3 are measured with an angular aperture of $\geq 0.5^\circ$. In advance, the dynamics of single speckles of the scattering pattern

#78429 - $15.00 USD Received 22 Dec 2006; revised 23 Mar 2007; accepted 26 Mar 2007; published 3 Apr 2007

was measured in the steady-state with a small angular aperture of $\leq$ 27". The results are shown in Fig. 4 and reveal quasi-periodic oscillations of the scattering intensity with specific periods for different scattering patterns. This temporal behavior is similar to that reported for $LiTaO_3$:Fe crystals [11].

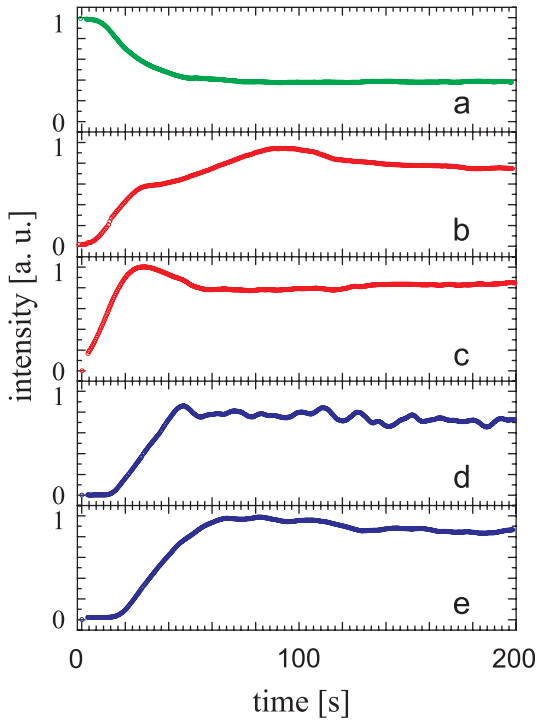

Fig. 3. Intensity kinetics of the pump beam (a), pattern i) (b), pattern ii) (c), pattern iii) (d), and of pattern iv) (e) with $\lambda = 532$ nm and I_p =0.5 W/cm^2.

4. Discussion

As it can be seen from Fig. 3, the scattering intensity first emerges from a very low initial level and then increases to the steady state for all four patterns, while the pump beam intensity simultaneously decreases. At the same time, the patterns show qualitatively different spatio-temporal properties and, hence, belong to different photo-induced processes. As it will be discussed in the following, they are all strongly related to the photo-induced response of $LiNbO_3$:Fe.

Patterns i)-iii) can be identified with previously reported types of scattering. However, their study is still not yet completed and further theoretical and experimental investigation is required. Pattern iv) is reported for the first time. As we will show, it is the result of a parametric wave-mixing process of coherent optical noise and the pump beam on the combination of photorefractively recorded phase-gratings and photo-induced ferroelectric structures. Some of the contributing processes are also involved in the formation of the first three patterns. In particular: frequency detuning as origin of the polarization-isotropic lobes, parametric wave-mixing yielding the polarization-anisotropic ring, and photo-induced formation of ferroelectric domains responsible for the polarization-isotropic line. Therefore, a discussion on the patterns i)-iii) will forego the analysis of the pattern iv). We will finally classify the corresponding scattering processes with respect to the role of the photorefractive effect. We consider a classic

#78429 - $15.00 USD Received 22 Dec 2006; revised 23 Mar 2007; accepted 26 Mar 2007; published 3 Apr 2007

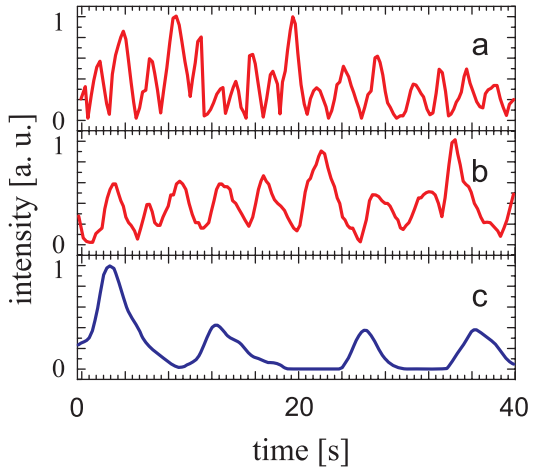

Fig. 4. Intensity dynamics of a single speckle of the scattering in the steady state: a) pattern i), b) pattern ii), and c) pattern iv).

definition of the photorefractive effect which includes photoexcitation of electric charge carriers into the conduction band, the formation of electric space-charge fields due to the migration of the carriers from brighter to darker regions of the light pattern via charge transport mechanisms (i.e. via the photovoltaic effect in $LiNbO_3$:Fe), and the modulation of the refractive index via the linear electrooptic effect.

4.1. Patterns i) to iii)

i) The first pattern is one of the most effective scattering phenomena almost always observed in photorefractive materials. It is usually interpreted as the result of the nonlinear amplified coherent optical noise emerged on optical inhomogeneities of the crystal. The amplification is due to two-wave mixing (2WM) processes on elementary photorefractive gratings recorded with the pump beam [12]. However, for $LiNbO_3$:Fe and other photorefractive materials with dominating photovoltaic effect this model has a principal drawback: The photovoltaic response for identically polarized waves results in a zero phase shift between the recorded photorefractive grating and the optical interference pattern. This does not permit the stationary energy exchange between the waves. Recently, the first approach to overcome this problem was presented considering small frequency shifts $\Delta\Omega = \omega_p - \omega_s$ between the pump beam and scattered waves. The frequency detunings $\Delta\Omega$ provide a permanent spatial mismatch between light and refractive-index patterns, that lifts the restrictions of the local response for the stationary amplification. The first experimental proof of this model was made for $LiTaO_3$:Fe, which possesses photovoltaic and photorefractive properties similar to those in $LiNbO_3$:Fe. Pronounced, quasi-periodic intensity fluctuations (or beatings) were observed in single speckles of the scattering pattern [11]. Such beatings are found in our samples of $LiNbO_3$:Fe, as well, as shown in Fig. 4(a). This result suggests the general importance of frequency detunings for scattering amplification processes. The intensity beatings can not be observed in Fig. 3(b) because of the integration of the multitude of different scattering components collected by the photodiode in a rather large angular interval.

The double-sided spatial shape of the pattern along the **c**-axis is defined by the photovoltaic charge-transport proportional to the photovoltaic tensor component β_{33}. However, the origin of the very pronounced maxima in the intensity distribution remains an open question, since the photovoltaic field does not depend on the grating period. The contribution of the diffusion

#78429 - $15.00 USD Received 22 Dec 2006; revised 23 Mar 2007; accepted 26 Mar 2007; published 3 Apr 2007

charge transport to the light amplification also requires careful examination.

The pattern i) is also called beam-fanning in the literature, according to the model approach proposed in Ref. [13], where the pattern is explained by self-defocussing of the pump beam on a photorefractive lens-like profile. However, we prefer the definitions related to photo-induced light scattering (PILS) [12]. In advance, to distinguish the pattern i) from other manifestations of the PILS phenomenon, we particularly identify it as the wide-angle polarization-isotropic PILS of $e-e$ type. As it was mentioned, the designation "polarization-isotropic" indicates that the pump and scattering waves have the same polarization, in particular extraordinary polarization as it is denoted by the corresponding "e" indices. The term "wide-angle" shows that it originates from the superposition of various elementary 2WM processes contributing to the light amplification, the resulting pattern has a shape of rather diffuse light lobes propagating in wide angular intervals.

ii) From the geometric point of view the ring in Fig. 2(a) is identified as the so-called parametric polarization-anisotropic PILS process of the $ee-eo$ type [14]. It was explained as the result of a four-wave mixing (4WM) process between two extraordinary pump waves (ee), and one extraordinary and one ordinary (eo) scattering waves. In the corresponding phase-matching conditions

$$\mathbf{k}^{\mathbf{e}}_{\mathbf{p1}} - \mathbf{k}^{\mathbf{o}}_{\mathbf{s2}} = \mathbf{k}^{\mathbf{e}}_{\mathbf{s1}} - \mathbf{k}^{\mathbf{e}}_{\mathbf{p2}} = \mathbf{K}_{12}, \tag{1}$$

wavevectors $\mathbf{k}^{\mathbf{e}}_{\mathbf{p1}}$ and $\mathbf{k}^{\mathbf{e}}_{\mathbf{p2}}$ denote two pump waves (for a single pump beam $\mathbf{k}^{\mathbf{e}}_{\mathbf{p1}} = \mathbf{k}^{\mathbf{e}}_{\mathbf{p2}} = \mathbf{k}^{\mathbf{e}}_{\mathbf{p}}$), $\mathbf{k}^{\mathbf{e}}_{\mathbf{s1}}$ and $\mathbf{k}^{\mathbf{o}}_{\mathbf{s2}}$ are wavevectors of extraordinary and ordinary scattering components, and $\mathbf{K}_{12}$ is the photorefractive grating, respectively. It should be noted that the grating recording by mutually orthogonal polarized waves is provided by the nondiagonal photovoltaic β^{a}_{15} and electrooptic r_{51} tensor components in $LiNbO_3$ doped with Cu or Fe. As it can be seen from Fig. 5, where the diagram of these vectors is plotted in the plane normal to the viewing screen, the term "parametric" means that the recording of the same photorefractive grating by different light waves results in an energy exchange. For instance, the scattering wave $\mathbf{k}^{\mathbf{o}}_{\mathbf{s2}}$ can be amplified via the diffraction of the pump wave $\mathbf{k}^{\mathbf{e}}_{\mathbf{p1}}$ on the grating $\mathbf{K}_{12}$ recorded by waves $\mathbf{k}^{\mathbf{e}}_{\mathbf{s1}}$ and $\mathbf{k}^{\mathbf{e}}_{\mathbf{p2}}$. The theoretical half-apex angle θ_s =26.62° calculated with the help of the diagram and refractive indices n_e, n_o taken from Ref. [15] is in perfect agreement with the experimental results.

Actually, the 4WM process described by Eq. (1) should result in two coincident and orthogonally polarized scattering rings (extraordinary and ordinary) with the pump beam in the center on the viewing screen. However, only the ordinarily polarized scattering (o-ring) is observed in the experiment. In $LiNbO_3$:Cu the depletion of the e-ring (corresponding to $\mathbf{k}^{\mathbf{e}}_{\mathbf{s1}}$ in Fig. 5) can be explained by an energy exchange between mutually orthogonal polarized waves via 2WM in the direction $e \rightarrow o$ defined by the sign of β^{a}_{15}. In $LiNbO_3$:Fe, β^{a}_{15} changes its sign which results in the change of the 2WM energy transfer to $o \rightarrow e$. However, the o-ring is still observed in the experiment, while the e-ring is missing. We believe that frequency detunings discussed for the wide-angle $e-e$ PILS, and which also are detected in our experiment for the parametric $ee-eo$ PILS, play an important role, here. The speckle-dynamics of the steady-state ring shows qualitatively similar quasi-periodic beatings (see Fig. 4(a), (b)). The comparison of these two dynamics further shows that the frequencies are different for $e-e$ and $ee-eo$ processes, which possibly results in the depletion of the e-ring. If the frequency detunings originate from temporal fluctuations of the photoelectric response of the crystal, as discussed in Ref. [16], then the value $\Delta\Omega$ is strongly dependent on the ratio between photovoltaic and diffusion contributions to the recording of the particular photorefractive grating. The $e-e$ process occurs only on gratings recorded by waves of equal polarization, while in the $ee-eo$ process also gratings recorded by mutually orthogonal polarized waves are involved. In the latter case, the recording occurs only due to the photovoltaic charge transport.

#78429 - $15.00 USD Received 22 Dec 2006; revised 23 Mar 2007; accepted 26 Mar 2007; published 3 Apr 2007

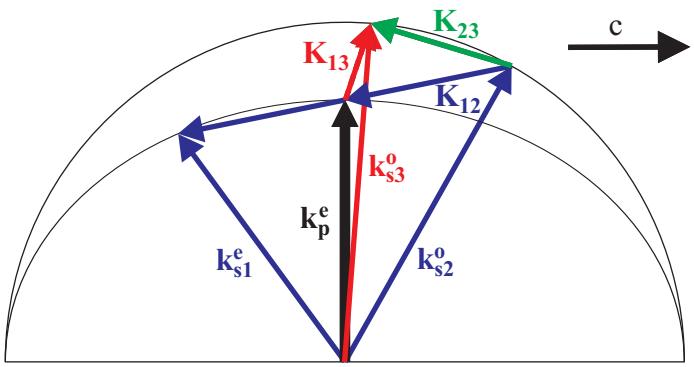

Fig. 5. The phase-matching diagram, in the plane parallel to the pump beam and the **c**-axis, explaining the appearance of the patterns ii) and iv).

iii) The third pattern, formed by the extra-ordinarily polarized scattering into the line crossing the pump beam ($e-$line), is a type of scattering different from PILS. However, it is related to the efficiency of the photorefractive electric charge transport in $LiNbO_3$. This scattering line emerges from polar structures (like ferroelectric 180°-domains) induced in the bulk via photovoltaic space-charge fields. Surface microdomains induced by light were already reported in *c*-cut samples of $LiNbO_3$:Fe according to predictions of Ref. [9]. The domains were visualized by conical light scattering [10]. It is suggested that very high photovoltaic fields ($\sim 10^5$ V/cm) are induced by the light between the crystal $+c$- and $-c$-faces due to electric currents proportional to the tensor component β_{33} or β_{31}, depending on the light polarization. 180°-domains nucleated on the crystal surface along the **c**-axis. Usually ferroelectric domains in $LiNbO_3$ are characterized by a needle-like shape with transversal dimensions much smaller than the longitudinal ones. The scattering from such structures is equivalent to the scattering from infinitely long, circular cylinders [17] and results in a scattering cone with axis colinear with the crystal's polar axis. It is clear, that the scattering will be visualized as a ring crossing the pump beam on a viewing screen. The characteristic feature of the scattering from photo-induced microdomains is the pronounced temporal threshold in the very beginning of the dynamics of the scattering, which determines the time necessary for the rise-up of the space-charge field to the value sufficient for domain nucleation.

In our experimental setup where *a*-cut samples are illuminated normally to the **c**-axis, the photovoltaic charge separation between large crystal surfaces is not possible because the corresponding photovoltaic β_{13}-currents are zero. We expect that ferroelectric domains are induced in the bulk on the rim of the illuminated region due to large photovoltaic β_{33}-currents. In this case the apex angle of the scattering cone equals 180° and the ring on the viewing screen is degenerated to a line perpendiculary to the **c**-axis. The time threshold as characteristic feature of scattering from photo-induced domains is observed for pattern iii) (see Fig. 3(d)). The line emerges only when the intensity of the $e-e$ scattering (which can be considered as a measure of the increase of the photovoltaic field in the crystal) is already very close to saturation. The angular width of the line is larger than the one of the $ee-eo$ ring, because the first one depends on the geometrical properties of photo-induced domains and the latter is defined by the phase-matching conditions shown in Fig. 5. The two following facts justify our assumption about the bulk origin of photo-induced domains responsible for the scattering into the line: a) the scattering does not disappear if the crystal is immersed in an electrically conductive fluid, b) the exposure for reaching the threshold does not depend on the crystal thickness. Taking all this into account, we assume that the *e*-line belongs to scattering from ferroelectric micro-domains

#78429 - $15.00 USD Received 22 Dec 2006; revised 23 Mar 2007; accepted 26 Mar 2007; published 3 Apr 2007

nucleated at the presence of bulk photovoltaic fields.

4.2. Parametric hybrid PILS involving light-induced ferroelectric structures

The geometrical analysis of the scattering pattern iv) consisting from two arcs shows that it can neither be only explained by 2WM or 4WM processes on photorefractive gratings like $e-e$ or $ee-eo$ patterns, nor via linear scattering from 180°-domains like the *e*-line. At the same time, the characteristic threshold feature of the temporal development (Fig. 3(e)) on one side, and the polarization-anisotropic character of the scattering on the other side, let us suggest that this pattern is a new type of scattering which is the result of the mixture of a parametric PILS process with the scattering from micro-scale structures in the crystal. A distinguishing geometric feature of the scattering pattern is the equal distance between the arcs and the closest part of the $ee-eo$ ring in the way that the same grating $\mathbf{K}_{23}$

$$\mathbf{K}_{23} = \mathbf{k}^{\mathbf{o}}_{\mathbf{s2}} - \mathbf{k}^{\mathbf{o}}_{\mathbf{s3}}, \tag{2}$$

can be recorded by different pairs of scattering waves, one from the ring ($\mathbf{k}^{\mathbf{o}}_{\mathbf{s2}}$) and the other from the arc ($\mathbf{k}^{\mathbf{o}}_{\mathbf{s3}}$), located on one vertical semi-plane above or beneath the pump beam. Deformations of the ring resulting from the tilting of the pump beam from the normal incidence will be followed by corresponding changes in the shape of arcs, because the conditions of Eq. (2) have to be kept. The upper and the lower arcs should undergo different changes as it was experimentally proven: The curvature of the part located in the tilting direction is increased, while the other part is decreased (see Fig. 2(b)).

The grating $\mathbf{K}_{23}$ can be also considered as the sum of the already discussed parametric grating $\mathbf{K}_{12}$ and of the new grating $\mathbf{K}_{13} = \mathbf{k}^{\mathbf{e}}_{\mathbf{p1}} - \mathbf{k}^{\mathbf{o}}_{\mathbf{s3}}$ between the arc scattering and the pump beam (see Fig. 5)

$$\mathbf{K}_{23} = \mathbf{K}_{12} + \mathbf{K}_{13}. \tag{3}$$

It is clear that different pairs of arcs can be created via phase-matching conditions with different gratings $\mathbf{K}_{23}$, made by various sets of waves $\mathbf{k}^{\mathbf{o}}_{\mathbf{s2}}$ and $\mathbf{k}^{\mathbf{o}}_{\mathbf{s3}}$. $\mathbf{K}_{12}$ and $\mathbf{k}^{\mathbf{o}}_{\mathbf{s2}}$ are specified by the $ee-eo$ process, and therefore the uniqueness of the pattern made with the help of the particular grating $\mathbf{K}_{23}$ should be related to the nature of $\mathbf{K}_{13}$ and $\mathbf{k}^{\mathbf{o}}_{\mathbf{s3}}$.

The approach of parametric wave mixing on pure photorefractive gratings fails to explain the preferable direction of the grating $\mathbf{K}_{13}$. The comparison of the two kinetics in Fig. 3(d), (e) indicates that light-induced domain structures should also be involved in the mixing, and $\mathbf{K}_{13}$ in this case is a measure of such structures. For instance, they can be related to domain nucleation on dislocation defects observed in $LiNbO_3$ at angles $25^\circ - 30^\circ$ from the **c**-axis [18]. This angular interval perfectly fits both the orientation of the grating $\mathbf{K}_{13}$ in the phase-matching diagram in Fig. 5 and the characteristic angular width (or diffuseness) of the arcs. It is reasonable to assume that photovoltaic β_{33}-currents cause the effective charge separation on dislocations and the resulting electric field induces domain nucleation. Although, ferroelectric domains slanted with respect to the **c**-axis are reported in $LiNbO_3$ [19], we will restrict the consideration only to the nucleation of ferroelectric domains along the **c**-axis in the following. However, even in this case domain tips make spatial sequences aligned in the dislocation directions, which can be read by the light because of local refractive-index variations following the nucleation process. The transverse dimension of ferroelectric domains in $LiNbO_3$ is typically varied from a few to dozen μm, which matches the calculated period $\Lambda \approx 6$ μm for the grating $\mathbf{K}_{13}$. Only the polarization-anisotropic diffraction on these microstructures resulting in $\mathbf{k}^{\mathbf{o}}_{\mathbf{s3}}$ can fulfill the phase-matching conditions given by Eqs. (2), (3). It can be suggested that the ferroelectric grating $\mathbf{K}_{13}$ can then be complemented by the photorefractive grating $\mathbf{K}_{13}$ recorded and afterwards

#78429 - $15.00 USD Received 22 Dec 2006; revised 23 Mar 2007; accepted 26 Mar 2007; published 3 Apr 2007

enhanced by wave mixing. To complete the picture, frequency detunings also should be taken into account for scattering amplification. According to the results of the comparative study of the single-speckle dynamics, the frequency detunings can be different for waves $\mathbf{k}_{s2}^{0}$ and $\mathbf{k}_{s3}^{0}$, which considerably complicates the analysis of scattering amplification processes.

According to the proposed model we can classify the pattern iv) as a parametric hybrid PILS where the scattering and pump beam are coupled via multi-wave mixing processes on a combination of photorefractive gratings and ferroelectric structures both induced in the crystal bulk by the coherent illumination. Here, we should note that the reported type of scattering is different from those observed in periodically poled $LiNbO_3$:Fe crystal [3, 4]. Here the angular selective scattering rises via 4WM extended by periodic structures of ferroelectric domains, which are already fabricated during the crystal growth [20]. In our case, both the photorefractive and ferroelectric structures are induced by the same coherent radiation and their spatial alignment features self-adjustment. We suggest that the discovered scattering is not the only manifestation of such hybrid PILS effect, and, hence, other manifestations will be found with different experimental conditions and other combinations of different types of photo-induced structures.

5. Conclusions

The multi-compound pattern of photo-induced light scattering induced by a single pump beam in iron-doped $LiNbO_3$ is experimentally studied. A parametric hybrid PILS phenomenon is discovered and interpreted as the result of multi-wave mixing of the pump beam with the scattered waves on the combination of photorefractive gratings and ferroelectric micro-structures induced by coherent irradiation in the crystal bulk. Furthermore, the comparative analysis of the intensity dynamics of different PILS phenomena shows that frequency detunings can be a rather general and important factor providing an effective scattering amplification, that is still not enough widely elucidated in literature.

We suggest that the new type of scattering also can be an useful tool for studying as-grown as well as photo-induced polar structures, because it offers a non-destructive analysis of the corresponding bulk structures without any additional chemical treatment of the material, like etching of crystal surfaces.

Acknowledgments

Financial Support by the Deutsche Forschungsgemeinschaft (DFG, projects IM 37/2-2, GRK 695 and TFB13-04) is gratefully acknowledged.

#78429 - $15.00 USD Received 22 Dec 2006; revised 23 Mar 2007; accepted 26 Mar 2007; published 3 Apr 2007